

Robust Multivariate Functional Control Chart

Christian Capezza¹, Fabio Centofanti ^{*1}, Antonio Lepore¹, and Biagio Palumbo¹

¹*Department of Industrial Engineering, University of Naples Federico II, Piazzale Tecchio 80, 80125, Naples, Italy*

Abstract

In modern Industry 4.0 applications, a huge amount of data is acquired during manufacturing processes that are often contaminated with anomalous observations in the form of both casewise and cellwise outliers. These can seriously reduce the performance of control charting procedures, especially in complex and high-dimensional settings. To mitigate this issue in the context of profile monitoring, we propose a new framework, referred to as robust multivariate functional control chart (RoMFCC), that is able to monitor multivariate functional data while being robust to both functional casewise and cellwise outliers. The RoMFCC relies on four main elements: (I) a functional univariate filter to identify functional cellwise outliers to be replaced by missing components; (II) a robust multivariate functional data imputation method of missing values; (III) a casewise robust dimensionality reduction; (IV) a monitoring strategy for the multivariate functional quality characteristic. An extensive Monte Carlo simulation study is performed to compare the RoMFCC with competing monitoring schemes already appeared in the literature. Finally, a motivating real-case study is presented where the proposed framework is used to monitor a resistance spot welding process in the automotive industry.

Keywords: Functional Data Analysis, Profile Monitoring, Statistical Process Control, Robust Estimation, Casewise and Cellwise Outliers

1 Introduction

Control charts are known as the main tools for statistical process monitoring (SPM), whose aim is to detect when the process is out-of-control (OC), i.e., when special causes of variation

^{*}Corresponding author. e-mail: fabio.centofanti@unina.it

act on it. On the contrary, when only common causes are present, the process is said to be in control (IC). The application of control charts in modern industrial applications must however turn into value the massive amounts of data collected at high frequency by modern data acquisition systems. Several examples may be found in the current Industry 4.0 framework, which is reshaping the format of measurements that can be gathered in manufacturing processes.

In many cases, the experimental measurements of the quality characteristic of interest are in fact characterized by complex and high dimensional formats that are well represented as one or multiple functional data (Ramsay and Silverman, 2005; Kokoszka and Reimherr, 2017) also referred to as profiles. The simplest approach for SPM through one or multiple functional quality characteristics is based on the extraction of scalar features from each profile observation and the application of classical multivariate SPM techniques (Montgomery, 2012). However, the feature extraction step is known to be problem specific, arbitrary, and possibly masking useful information. Thus, this issue stimulated a growing interest in *profile monitoring* (Noorossana et al., 2011) that is the monitoring of a process through quality characteristic observations in the form of one or multiple profiles. Some recent examples of profile monitoring applications can be found in Menafooglio et al. (2018); Capezza et al. (2020, 2021a,b, 2022); Centofanti et al. (2021b).

Control charts are currently implemented in two phases. The first is referred to as Phase I and is concerned to identify a clean data set to be assumed as representative of the IC state of the process, named Phase I sample or Phase I observations. This data set is then used to quantify the expected variation of a future observation to be used for the prospective process monitoring, referred to as Phase II. Unfortunately, the identification of a Phase I sample in high-dimensional contexts is not an easy task due to the large presence of outlying observations in at least one component of a multivariate functional quality characteristic. On the other hand, control charts are very sensitive to the presence of outlying observations in the Phase I sample that inflate control limits and, therefore, reduce the detection power in Phase II.

In this view, let us consider the real-case study on the SPM of a resistance spot welding (RSW) process in the automotive body-in-white manufacturing that motivated this re-

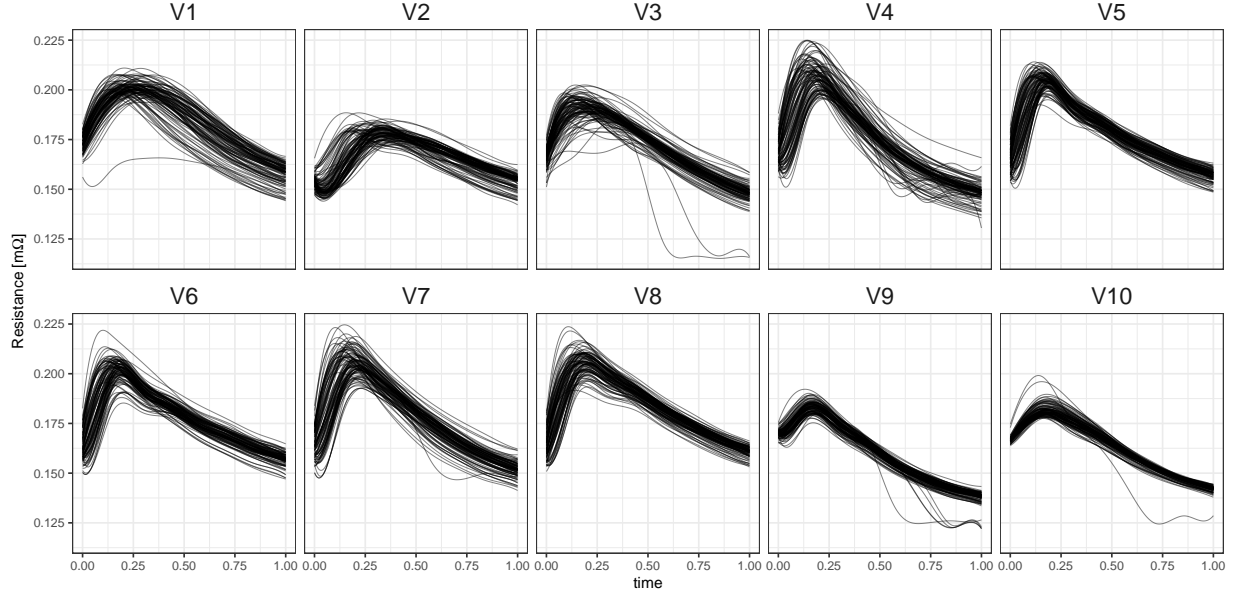


Figure 1: Sample of 100 DRCs, measured in $m\Omega$, that are acquired during the RSW process from the real-case study in Section 4. The different panels refer to the corresponding different spot welds, denoted with names from V1 to V10.

search and will be thoroughly presented in Section 4. RSW is the most common technique employed in joining metal sheets, mainly because it guarantees the structural integrity and solidity of welded items while being adaptable for mass production (Martín et al., 2014). Among on-line measurements of RSW process parameters, the so-called dynamic resistance curve (DRC) is recognized as the full technological signature of the metallurgical development of a spot weld (Dickinson et al., 1980; Capezza et al., 2021b) and, thus, it can be regarded as an in-line low-cost proxy of the RSW process quality with respect to off-line costly destructive tests. For illustrative purposes, each panel of Figure 1 displays 100 multivariate DRCs randomly sampled from the real-case study data set, measured in $m\Omega$, acquired during RSW lab tests at Centro Ricerche Fiat (Italy) and refers to the same spot weld locations on 100 different items. Figure 1 clearly highlights the motivating challenge of handling outliers possibly occurring in a few components (i.e., panels) and different items.

SPM methods use two common alternatives to deal with outliers, namely the *diagnostic* and the *robust* approaches (Kruger and Xie, 2012; Hubert et al., 2015). The diagnostic approach is based on standard statistics after the removal of sample units identified as outliers that translates into SPM methods where iterative re-estimation procedures are considered in Phase I. This approach could be often safely applied to eliminate the effect

of a small number of very extreme observations In the Phase I sample. However, this approach may fail to detect moderate outliers that are not always as easy to label correctly. On the contrary, the robust approach accepts all the data points by means of a robust estimator that reduces the impact of outliers on the final results (Maronna et al., 2019). Throughout this paper, the term *robust* means “outlier resistant” and not “robust to model misspecification” as it is sometimes used in the literature. Under the robust approach, the terms Phase I sample or Phase I observations will be used as before to refer to the data set representative of the IC state even though it may be contaminated by outliers.

In the SPM literature, several robust approaches have been proposed for monitoring a multivariate scalar quality characteristic. Alfaro and Ortega (2009) show a comparison of robust alternatives to the classical Hotelling’s control chart. They include two alternative Hotelling’s T^2 -type control charts for individual observations, proposed by Vargas (2003) and Jensen et al. (2007), based on the minimum volume ellipsoid and the minimum covariance determinant estimators (Rousseeuw, 1984), respectively. Moreover, the comparison includes the control chart based on the reweighted minimum covariance determinant estimators, proposed by Chenouri et al. (2009). More recently, Cabana and Lillo (2021) propose a robust Hotelling’s T^2 procedure using the robust shrinkage reweighted estimator. To the best of the authors’ knowledge, Kordestani et al. (2020) and Moheghi et al. (2020) are the only ones to propose robust estimators to monitor simple linear profiles, which are not able to capture the functional nature of a multivariate functional quality characteristic.

Beyond the SPM literature, several works have been proposed to deal with outlying functional observations. The classical L-estimator, which is the linear combination type estimator (Maronna et al., 2019), is extended to the functional data setting to robustly estimate the center of a functional distribution through trimming (Fraiman and Muniz, 2001; Cuesta-Albertos and Fraiman, 2006) and functional data depths (Cuevas and Fraiman, 2009; López-Pintado and Romo, 2011). Sinova et al. (2018) introduce in the same setting the notion of maximum-likelihood type estimator, referred to as M-estimator. More recently, Centofanti et al. (2021a) propose a robust functional analysis of variance (ANOVA) that reduces the weights of outlying functional data on the results of the analysis.

Robust approaches appeared also in functional principal component analysis (FPCA)

and are classified by Boente and Salibián-Barrera (2021) in three groups, based on the specific property enjoyed by the resulting principal components. Methods in the first group perform the eigenanalysis of a robust estimator of the scatter operator, as the spherical principal components method of Locantore et al. (1999) and the indirect approach of Sawant et al. (2012). The latter performs a robust PCA method (e.g., the ROBPCA proposed by Hubert et al. (2005)) on the matrix of the basis coefficients corresponding to a basis expansion representation of the functional data. The second group contains projection-pursuit approaches as the one proposed by Hyndman and Ullah (2007), that sequentially search for the directions that maximize a robust estimator of the spread of the data projections. The third group is composed of methods that estimate the principal component space by minimizing a robust reconstruction error measure (Lee et al., 2013). Additionally, it is worth mentioning diagnostic approaches for functional outlier detection for both univariate (Hyndman and Shang, 2010; Arribas-Gil and Romo, 2014) and multivariate functional data (Hubert et al., 2015; Alemán-Gómez et al., 2022).

In presence of many functional variables, the curse of dimensionality exacerbates the development of scalable robust approaches. In fact, traditional multivariate robust estimators assume only a so-called *casewise* contamination model for the data, which consists of a mixture of two distributions, one representing the majority of the cases that are free of contamination and the second describing the minority of the cases assumed as generated by an unspecified outlier distribution. These traditional estimators work well when a small number of cases are contaminated. However, they are affected by the outlier propagation problem (Alqallaf et al., 2009) and may fail when the fraction of perfectly observed cases is small. Unfortunately, this is very common when the data are high dimensional and outliers are *cellwise*, that is contamination in each variable is independent of the other ones.

Moreover, as pointed out by Agostinelli et al. (2015), in the multivariate scalar setting, casewise and cellwise data contamination may occur together. To overcome this problem, they propose a two steps method. In the first step, they use a univariate filter to detect large cellwise outliers and replace them with missing values. Then, in the second step, a robust estimation specifically designed to deal with missing data is applied to the incomplete data to overcome the casewise contamination. Leung et al. (2016) notice however that

the univariate filter does not handle moderate-size cellwise outliers well and introduce in the first step of Agostinelli et al. (2015) a consistent bivariate filter in combination with the univariate filter. Rousseeuw and Bossche (2018) propose a new method for detecting deviating data cells that takes into account variables correlation, whereas, Tarr et al. (2016) devise a method for robust estimation of precision matrices under cellwise contamination.

In this paper, we propose a new framework, referred to as robust multivariate functional control chart (RoMFCC), for the SPM of multivariate functional data that is robust to both functional casewise and cellwise outliers. As detailed in Section 2, to deal with the latter, the proposed framework considers an extension of the filtering approach proposed by Agostinelli et al. (2015) for univariate functional data and an imputation method inspired by the robust imputation technique of Branden and Verboven (2009). Moreover, it also considers a robust multivariate functional principal component analysis (RoMFPCA) based on the ROBPCA method (Hubert et al., 2005), and a profile monitoring strategy built on the Hotelling’s T^2 and the squared prediction error (SPE) control charts (Noorossana et al., 2011; Grasso et al., 2016; Centofanti et al., 2021b; Capezza et al., 2020, 2021a, 2022).

A Monte Carlo simulation study is performed in Section 3 to compare the RoMFCC with competing monitoring schemes that already appeared in the literature based on the ability in Phase II of detecting a process mean shift, where the Phase I sample is contaminated by casewise and cellwise outliers in different scenarios and severity levels. The practical applicability of the proposed control chart is illustrated in Section 4 by means of the motivating real-case study introduced above. Section 5 concludes the article. Supplementary Materials are available online and contain details on data generation in the simulation study and additional simulation results. All computations and plots have been obtained using the programming language R (R Core Team, 2021).

2 The Robust Multivariate Functional Control Chart Framework

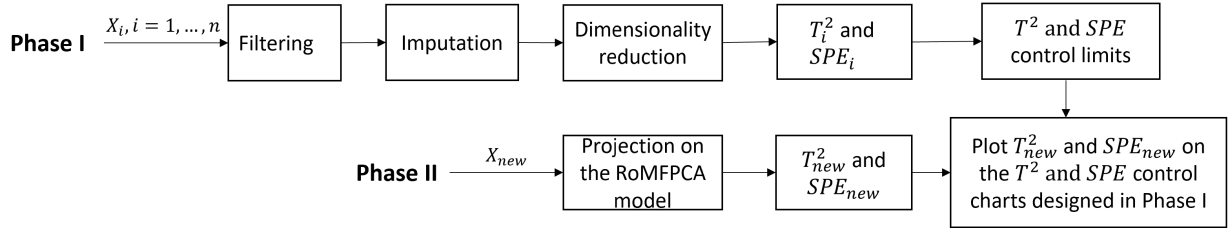
The proposed RoMFCC is a new general framework for the SPM of multivariate functional data and is able to deal with both Phase I functional casewise and cellwise outliers. It

relies on the following four main elements:

- (I) *functional univariate filter* is used to identify functional cellwise outliers and replace them by missing component values;
- (II) *robust multivariate functional data imputation* to replace missing values;
- (III) *casewise robust dimensionality reduction* to reduce the infinite dimensionality of the multivariate functional data that is robust to casewise outliers;
- (IV) *monitoring strategy* of the process through the multivariate functional data obtained as the output of the previous steps.

These elements are combined in the proposed RoMFCC framework in a Phase II monitoring strategy described in the scheme of Figure 2, where a set of Phase I observations \mathbf{X}_i , $i = 1, \dots, n$ of the multivariate functional quality characteristic \mathbf{X} , which can be contaminated with outliers, is used for the design of the control chart.

Figure 2: Scheme of the RoMFCC framework.



In what follows, we describe a specific implementation of the RoMFCC framework. In the *filtering* step, we propose a (I) functional univariate filter, which is named as FUF and is an extension of the filtering stage of Agostinelli et al. (2015) to identify functional cellwise outliers and replace them by missing components. and, then, replaced by missing components. In the *imputation* step, these are then imputed through a new (II) robust functional data imputation, which is named RoMFDI and is based on the technique of Branden and Verboven (2009). Once the imputed Phase I sample is obtained, it is used to estimate the RoMFPCA model, which is considered as the casewise robust dimensionality reduction method, and perform the (III) *casewise robust dimensionality reduction* step. The Hotelling's T^2 and SPE statistics of the (IV) monitoring strategy as well as their control limits are, then, computed. In Phase II, each new observation X_{new} is projected on the RoMFPCA model to compute the values of the Hotelling's T^2 and SPE statistics according

to the model identified in Phase I and referred to as T_{new}^2 and SPE_{new} , respectively. An alarm signal is issued if either T_{new}^2 or SPE_{new} violates the corresponding control limit. Note that, when the sample size n is small compared to the number of process variables, an undesirable effect upon the performance of the RoMFCC could arise (Ramaker et al., 2004; Kruger and Xie, 2012). Strictly speaking, to prevent overfitting issues that could reduce the monitoring performance of the RoMFCC, the Phase I sample is randomly split into non-overlapping sets, referred to as *training* and *tuning* sets. The former is used to estimate the RoMFPCA model, whereas the latter is considered to estimate the T^2 and SPE control limits.

The RoMFPCA is presented in Section 2.1. Then, Section 2.2, Section 2.3, and, Section 2.4 describe the FUF, the RoMFDI method, and the monitoring strategy, respectively.

2.1 Robust Multivariate Functional Principal Component Analysis

Let $L^2(\mathcal{T})$ denote the Hilbert space of square integrable functions defined on the compact set $\mathcal{T} \in \mathbb{R}$, with the inner product of two functions $f, g \in L^2(\mathcal{T})$ given by $\langle f, g \rangle = \int_{\mathcal{T}} f(t) g(t) dt$, and the norm $\|\cdot\| = \sqrt{\langle \cdot, \cdot \rangle}$. Let $\mathbf{X} = (X_1, \dots, X_p)^T$ be a random vector with realizations in the Hilbert space \mathbb{H} of p -dimensional vectors of $L^2(\mathcal{T})$ functions, with the inner product of two function vectors $\mathbf{f} = (f_1, \dots, f_p)^T$ and $\mathbf{g} = (g_1, \dots, g_p)^T$ in \mathbb{H} given by $\langle \mathbf{f}, \mathbf{g} \rangle_{\mathbb{H}} = \sum_{j=1}^p \langle f_j, g_j \rangle$ and the norm $\|\cdot\|_{\mathbb{H}} = \sqrt{\langle \cdot, \cdot \rangle_{\mathbb{H}}}$.

We assume that \mathbf{X} has mean $\boldsymbol{\mu} = (\mu_1, \dots, \mu_p)^T$, where $\mu_j(t) = E(X_j(t))$, $j = 1, \dots, p$, $t \in \mathcal{T}$ and covariance $\mathbf{G} = \{G_{jk}\}_{1 \leq j, k \leq p}$, $G_{jk}(s, t) = \text{Cov}(X_j(s), X_k(t))$, $s, t \in \mathcal{T}$. In what follows, differences in variability and unit of measurement among X_1, \dots, X_p , are taken into account by using the transformation approach of Chiou et al. (2014), that is we replace \mathbf{X} with the vector of standardized variables $\mathbf{Z} = (Z_1, \dots, Z_p)^T$, where $Z_j(t) = v_j(t)^{-1/2}(X_j(t) - \mu_j(t))$, with $v_j(t) = G_{jj}(t, t)$, $j = 1, \dots, p$, $t \in \mathcal{T}$. Then, from the multivariate Karhunen-Loève's theorem (Happ and Greven, 2018) it follows that

$$\mathbf{Z}(t) = \sum_{l=1}^{\infty} \xi_l \boldsymbol{\psi}_l(t), \quad t \in \mathcal{T},$$

where $\xi_l = \langle \boldsymbol{\psi}_l, \mathbf{Z} \rangle_{\mathbb{H}}$ are random variables, say *principal components scores* or simply *scores*, such that $E(\xi_l) = 0$ and $E(\xi_l \xi_m) = \lambda_l \delta_{lm}$, with δ_{lm} the Kronecker delta. The elements of the orthonormal set $\{\boldsymbol{\psi}_l\}$, $\boldsymbol{\psi}_l = (\psi_{l1}, \dots, \psi_{lp})^T$, with $\langle \boldsymbol{\psi}_l, \boldsymbol{\psi}_m \rangle_{\mathbb{H}} = \delta_{lm}$, are referred to as *principal components*, and are the eigenfunctions of the covariance \mathbf{C} of \mathbf{Z} corresponding to the eigenvalues $\lambda_1 \geq \lambda_2 \geq \dots \geq 0$. Following the approach of Ramsay and Silverman (2005), the eigenfunctions and eigenvalues of the covariance \mathbf{C} are estimated through a basis function expansion approach. Specifically, we assume that each function Z_j and eigenfunction $\boldsymbol{\psi}_l$ of \mathbf{C} with components ψ_{lj} , for $j = 1, \dots, p$, $l = 1, \dots, \infty$, can be approximated by the following finite sums of K terms

$$Z_j(t) \approx \sum_{k=1}^K c_{jk} \phi_{jk}(t), \quad \psi_{lj}(t) \approx \sum_{k=1}^K b_{lj} \phi_{jk}(t), \quad t \in \mathcal{T}. \quad (1)$$

That is, Z_j and ψ_{lj} are approximated as linear combinations of the components of a K -dimensional vector of basis functions $\boldsymbol{\phi}_j = (\phi_{j1}, \dots, \phi_{jK})^T$, with coefficient vectors $\mathbf{c}_j = (c_{j1}, \dots, c_{jK})^T$ and $\mathbf{b}_{lj} = (b_{lj1}, \dots, b_{ljK})^T$, respectively. With these assumptions, standard multivariate functional principal component analysis (Ramsay and Silverman, 2005; Chiou et al., 2014) estimates eigenfunctions and eigenvalues of the covariance \mathbf{C} by performing standard multivariate principal component analysis on the random vector $\mathbf{W}^{1/2} \mathbf{c}$, where $\mathbf{c} = (\mathbf{c}_1^T, \dots, \mathbf{c}_p^T)^T$ and \mathbf{W} is a block-diagonal matrix with diagonal blocks \mathbf{W}_j , $j = 1, \dots, p$, whose entries are $\langle \phi_{jk_1}, \phi_{jk_2} \rangle$, $k_1, k_2 = 1, \dots, K$. Then, the eigenvalues λ_l of \mathbf{C} are estimated by those of the covariance matrix of $\mathbf{W}^{1/2} \mathbf{c}$, whereas, the components $\psi_{l1}, \dots, \psi_{lp}$ of the corresponding eigenfunction $\boldsymbol{\psi}_l$ are estimated through Equation (1) with $\mathbf{b}_{lj} = \mathbf{W}^{-1/2} \mathbf{u}_{lj}$, where $\mathbf{u}_l = (\mathbf{u}_{l1}^T, \dots, \mathbf{u}_{lp}^T)^T$ is the eigenvector of the covariance matrix of $\mathbf{W}^{1/2} \mathbf{c}$ corresponding to λ_l . However, it is well known that standard multivariate principal component analysis is not robust to outliers (Maronna et al., 2019), which obviously reflects on the functional principal component analysis by probably providing misleading results. Extending the approach of Sawant et al. (2012) for multivariate functional data, the proposed RoMFPCA applies a robust principal component analysis alternative to the random vector $\mathbf{W}^{1/2} \mathbf{c}$. Specifically, we consider the ROBPCA approach of Hubert et al. (2005), which is a computationally efficient method explicitly conceived to produce estimates with

a high breakdown in high dimensional data settings and is commonly adopted in the functional context to handle a large percentage of contamination. Thus, given n independent realizations $\mathbf{X}_1, \dots, \mathbf{X}_n$ of \mathbf{X} , dimensionality reduction is achieved by approximating \mathbf{X}_i through $\hat{\mathbf{X}}_i$, for $i = 1, \dots, n$, as

$$\hat{\mathbf{X}}_i(t) = \hat{\boldsymbol{\mu}}(t) + \hat{\mathbf{D}}(t) \sum_{l=1}^L \hat{\xi}_{il} \hat{\boldsymbol{\psi}}_l(t) \quad t \in \mathcal{T} \quad (2)$$

where $\hat{\mathbf{D}}$ is a diagonal matrix whose diagonal entries are robust estimates $\hat{v}_j^{1/2}$ of $v_j^{1/2}$, $\hat{\boldsymbol{\mu}} = (\hat{\mu}_1, \dots, \hat{\mu}_p)^T$ is a robust estimate of $\boldsymbol{\mu}$, $\hat{\boldsymbol{\psi}}_l$, $l = 1, \dots, L$, are the first L robustly estimated principal components and $\hat{\xi}_{il} = \langle \hat{\boldsymbol{\psi}}_l, \hat{\mathbf{Z}}_i \rangle_{\mathbb{H}}$ are the corresponding scores with robustly estimated variances $\hat{\lambda}_l$. The estimates $\hat{\boldsymbol{\psi}}_l$ and $\hat{\lambda}_l$ are obtained through the n realizations of \mathbf{Z}_i estimated as $\hat{\mathbf{Z}}_i = \hat{v}_j^{-1/2}(\mathbf{X}_i - \hat{\boldsymbol{\mu}}_i)$ by using $\hat{\mu}_j$ and \hat{v}_j . The robust estimates $\hat{\mu}_j$ and \hat{v}_j are obtained through the scale equivariant functional M -estimator and the functional normalized median absolute deviation estimator proposed by Centofanti et al. (2021a). As in the multivariate setting, L is generally chosen such that the retained principal components $\hat{\boldsymbol{\psi}}_1, \dots, \hat{\boldsymbol{\psi}}_L$ explain at least a given percentage of the total variability, which is usually in the range 70-90%. However, more sophisticated methods could be used as well (see Jolliffe (2011) for further details).

2.2 Functional Univariate Filter

To extend the filter of Agostinelli et al. (2015) and Leung et al. (2016) to univariate functional data, let us consider n independent realizations $\mathbf{X}_1, \dots, \mathbf{X}_n$ of a random function X whose realizations are in $L^2(\mathcal{T})$. The proposed FUF considers the functional distances

$$D_i^{\text{fil}} = \sum_{l=1}^{L^{\text{fil}}} \frac{(\hat{\xi}_{il}^{\text{fil}})^2}{\hat{\lambda}_l^{\text{fil}}}, \quad i = 1, \dots, n, \quad (3)$$

where the estimated scores $\hat{\xi}_{il}^{\text{fil}} = \langle \hat{\boldsymbol{\psi}}_l^{\text{fil}}, \hat{\mathbf{Z}}_i \rangle$, eigenvalues $\hat{\lambda}_l^{\text{fil}}$, principal components $\hat{\boldsymbol{\psi}}_l^{\text{fil}}$, and standardized observations $\hat{\mathbf{Z}}_i$ of X_i are obtained by applying, with $p = 1$, the proposed RoMFPCA described in Section 2.1 to the sample X_1, \dots, X_n . In this setting, the RoMFPCA is suitably used to represent distances among X_i 's and not to perform dimensionality

reduction, thus L^{fil} should be sufficiently large to capture a large percentage of the total variability δ^{fil} . Let G_n be the empirical cumulative distribution function (cdf) of D_i^{fil} , i.e.,

$$G_n(x) = \frac{1}{n} \sum_{i=1}^n I(D_i^{\text{fil}} \leq x), \quad x \geq 0,$$

where $I(\cdot)$ denotes the indicator function. Then, a functional observation X_i is labeled as a cellwise outlier by comparing $G_n(x)$ with $G(x)$, $x \geq 0$, where G is the reference cdf for D_i^{fil} . Following Leung et al. (2016), we consider D_i^{fil} distributed as a chi-squared random variable with L^{fil} degrees of freedom, i.e., $D_i^{\text{fil}} \sim \chi_{L^{\text{fil}}}^2$. The proportion of flagged cellwise outliers is defined by

$$d_n = \sup_{x \geq \eta} \{G(x) - G_n(x)\}^+,$$

where $\{a\}^+$ represents the positive part of a , and $\eta = G^{-1}(\alpha)$ is a large quantile of D_i^{fil} . As Agostinelli et al. (2015), we set $\alpha = 0.95$. Finally, we flag $\lfloor nd_n \rfloor$ observations with the largest functional distances D_i^{fil} as functional cellwise outliers, where $\lfloor \cdot \rfloor$ denotes the floor function. From the arguments in Agostinelli et al. (2015) and Leung et al. (2016) the proposed FUF is consistent even when the actual distribution of D_i^{fil} is unknown. That is, when the tail of G is heavier than or equal to that of the actual unknown distribution, it will flag a cellwise outlier asymptotically correctly.

2.3 Robust Multivariate Functional Data Imputation

Let us consider the setting where the n independent realizations $\mathbf{X}_i = (X_{i1}, \dots, X_{ip})^T$, $i = 1, \dots, n$, of the multivariate functional quality characteristic \mathbf{X} may present missing components, i.e., for some i , at least one among X_{i1}, \dots, X_{ip} is missing. Let us assume that there is a set S_c of $c < n$ realizations with no missing component. As the robust imputation approach of Branden and Verboven (2009), the RoMFDI is a sequential imputation method. It starts from any observation $\mathbf{X}_{\underline{i}} \notin S_c$ having the smallest number, say s , of missing components. For notational convenience and without loss of generality, let us arrange the p components of $\mathbf{X}_{\underline{i}} = ((\mathbf{X}_{\underline{i}}^{\text{m}})^T, (\mathbf{X}_{\underline{i}}^{\text{o}})^T)^T$ such that the first s missing components are in the vector $\mathbf{X}_{\underline{i}}^{\text{m}}$, while the remaining $p - s$ observed ones are in $\mathbf{X}_{\underline{i}}^{\text{o}}$. The standardized version of $\mathbf{X}_{\underline{i}}$ is partitioned as $\hat{\mathbf{Z}}_{\underline{i}} = ((\hat{\mathbf{Z}}_{\underline{i}}^{\text{m}})^T, (\hat{\mathbf{Z}}_{\underline{i}}^{\text{o}})^T)^T$, where $\hat{\mathbf{Z}}_{\underline{i}}^{\text{m}}$ and $\hat{\mathbf{Z}}_{\underline{i}}^{\text{o}}$ are the standardized

versions of $\mathbf{X}_{\underline{i}}^m$ and $\mathbf{X}_{\underline{i}}^o$, respectively. By Equation (1), $\hat{\mathbf{Z}}_{\underline{i}}$ is uniquely identified by the Kp -dimensional coefficient vector $\mathbf{c}_{\underline{i}} = ((\mathbf{c}_{\underline{i}}^m)^T, (\mathbf{c}_{\underline{i}}^o)^T)^T$ related to the basis expansions of its p components, where K is the number of basis functions as in Equation (1). Therefore, the imputation of $\mathbf{X}_{\underline{i}}^m$ reduced to the imputation of $\mathbf{c}_{\underline{i}}^m$. We do this by minimizing the distance of $\mathbf{X}_{\underline{i}}$ from the space generated by the observations in S_c

$$\sum_{l=1}^{L^{\text{imp}}} \frac{(\hat{\xi}_{il}^{\text{imp}})^2}{\hat{\lambda}_l^{\text{imp}}}, \quad (4)$$

where $\hat{\xi}_{il}^{\text{imp}} = \langle \hat{\boldsymbol{\psi}}_l^{\text{imp}}, \hat{\mathbf{Z}}_{\underline{i}} \rangle_{\mathbb{H}}$, with principal components $\hat{\boldsymbol{\psi}}_l^{\text{imp}} = (\hat{\psi}_{l1}^{\text{imp}}, \dots, \psi_{lp}^{\text{imp}})^T$ and corresponding eigenvalues $\hat{\lambda}_l^{\text{imp}}$ obtained by applying RoMFPCA on the complete realizations in S_c , as in Section 2.1. The number L^{imp} of components is chosen sufficiently large to capture the desired percentage of the total variability δ^{imp} . Since principal components $\hat{\psi}_{lj}^{\text{imp}}$ are uniquely identified by their basis coefficients $\hat{\mathbf{b}}_{lj}$, $l = 1, \dots, L^{\text{imp}}$, $j = 1, \dots, p$, which can be arranged into the matrix $\hat{\mathbf{B}}$ having columns $\hat{\mathbf{b}}_l = (\hat{\mathbf{b}}_{l1}^T, \dots, \hat{\mathbf{b}}_{lp}^T)^T$, the objective function (4) can be calculated as $\mathbf{c}_{\underline{i}}^T \mathbf{C} \mathbf{c}_{\underline{i}}$, where the $Kp \times Kp$ matrix \mathbf{C} is

$$\mathbf{C} = \mathbf{W} \hat{\mathbf{B}} \hat{\boldsymbol{\Lambda}}^{-1} \hat{\mathbf{B}}^T \mathbf{W} = \begin{pmatrix} \mathbf{C}^{\text{m,m}} & \mathbf{C}^{\text{m,o}} \\ (\mathbf{C}^{\text{m,o}})^T & \mathbf{C}^{\text{o,o}} \end{pmatrix},$$

where \mathbf{W} is the block-diagonal matrix defined in Section 2.1 and $\hat{\boldsymbol{\Lambda}}$ the diagonal matrix whose diagonal entries are $\hat{\lambda}_l^{\text{imp}}$, $l = 1, \dots, L^{\text{imp}}$. The upper left $Ks \times Ks$ block $\mathbf{C}^{\text{m,m}}$ of \mathbf{C} contains the elements of \mathbf{C} corresponding to the missing components, while $\mathbf{C}^{\text{m,o}}$ represents the part of \mathbf{C} with the missing components in the rows and the observed components in the columns. The solution that minimizes the objective function (4) with respect to $\mathbf{c}_{\underline{i}}^m$ is

$$\hat{\mathbf{c}}_{\underline{i}}^m = \underset{\mathbf{c}_{\underline{i}}^m}{\text{argmin}} \left((\mathbf{c}_{\underline{i}}^m)^T, (\mathbf{c}_{\underline{i}}^o)^T \right)^T \mathbf{C} \left((\mathbf{c}_{\underline{i}}^m)^T, (\mathbf{c}_{\underline{i}}^o)^T \right)^T = -(\mathbf{C}^{\text{m,m}})^+ \mathbf{C}^{\text{m,o}} \mathbf{c}_{\underline{i}}^o, \quad (5)$$

where $(\mathbf{C}^{\text{m,m}})^+$ is the Moore-Penrose inverse of $\mathbf{C}^{\text{m,m}}$.

In order to overcome the correlation bias issue typical of deterministic imputation approaches (Little and Rubin, 2019; Van Buuren, 2018), we propose a stochastic imputation

method by imputing $\mathbf{c}_{\underline{i}}^{\text{m}}$ with

$$\mathbf{c}_{\underline{i}}^{\text{imp}} = \hat{\mathbf{c}}_{\underline{i}}^{\text{m}} + \boldsymbol{\varepsilon}_{\underline{i}}, \quad (6)$$

where $\boldsymbol{\varepsilon}_{\underline{i}}$ is a multivariate normal random variable with mean zero and covariance matrix robustly estimated (e.g., using the Rocke type estimator (Rocke, 1996)) based on the regression residuals of the coefficient vectors of the missing component on those of the observed components using the observations in S_c through the model in Equation (5). Accordingly, the components of $\hat{\mathbf{Z}}_{\underline{i}}^{\text{m}}$ are imputed with $\hat{\mathbf{Z}}_{\underline{i}}^{\text{imp}}$, whose j -th component is

$$\hat{Z}_{ij}^{\text{imp}}(t) = \left(\mathbf{c}_{ij}^{\text{imp}} \right)^T \boldsymbol{\phi}_j(t), \quad t \in \mathcal{T}, \quad j = 1, \dots, s,$$

where $\mathbf{c}_{ij}^{\text{imp}}$ is the vector of the elements of $\mathbf{c}_{\underline{i}}^{\text{imp}}$ corresponding to the j -th component of $\hat{\mathbf{Z}}_{\underline{i}}$ and $\boldsymbol{\phi}_j$ is defined as in Equation (1). The imputed values of $\mathbf{X}_{\underline{i}}^{\text{m}}$ are finally obtained by unstandardizing $\hat{\mathbf{Z}}_{\underline{i}}^{\text{imp}}$, and $\mathbf{X}_{\underline{i}}$ is then added to S_c . The whole imputing step described for $\mathbf{X}_{\underline{i}}$ is repeated iteratively until all missing observations are imputed. Observations where all components are missing, i.e., $s = p$, are trivially removed from the sample because their imputation does not provide any additional information for the analysis.

However, similarly to Branden and Verboven (2009), if the cardinality of S_c at the first iteration is sufficiently large, we suggest not updating the RoMFPCA model at each iteration. To take into account the increased noise due to single imputation, the proposed RoMFDI can be easily included in a multiple imputation framework (Van Buuren, 2018; Little and Rubin, 2019). It is worth explicitly noting that, due to the presence of the stochastic component $\boldsymbol{\varepsilon}_{\underline{i}}$ in Equation (6), the imputed data set is not deterministically assigned. Therefore, by performing several times the RoMFDI in the imputation step of the RoMFCC implementation, the corresponding multiple estimated RoMFPCA models could be combined by averaging the robustly estimated covariance functions, thus performing a multiple imputation strategy as suggested by Van Ginkel et al. (2007).

2.4 The Monitoring Strategy

The last (IV) element of the proposed RoMFCC implementation relies on the consolidated monitoring strategy for a multivariate functional quality characteristic \mathbf{X} based on

Hotelling's T^2 and SPE control charts. The former assesses the stability of \mathbf{X} in the finite dimensional space spanned by the first principal components identified through the RoMF-PCA (Section 2.1), whereas, the latter monitors changes along directions in the complement space. Specifically, the Hotelling's T^2 statistic for \mathbf{X} is defined as

$$T^2 = \sum_{l=1}^{L^{\text{mon}}} \frac{(\xi_l^{\text{mon}})^2}{\lambda_l^{\text{mon}}},$$

where λ_l^{mon} are the variances of the scores $\xi_l^{\text{mon}} = \langle \boldsymbol{\psi}_l^{\text{mon}}, \mathbf{Z} \rangle_{\mathbb{H}}$, \mathbf{Z} is the vector of standardized variable corresponding to \mathbf{X} and $\boldsymbol{\psi}_l^{\text{mon}}$ is the vector of principal components as defined in Section 2.1. The number L^{mon} is chosen such that the retained principal components explain at least a given percentage δ^{mon} of the total variability. The statistic T^2 is the standardized squared distance from the center of the orthogonal projection of \mathbf{Z} onto the principal component space spanned by $\boldsymbol{\psi}_1^{\text{mon}}, \dots, \boldsymbol{\psi}_{L^{\text{mon}}}^{\text{mon}}$. Whereas, the distance between \mathbf{Z} and its orthogonal projection onto the principal component space is measured through the SPE statistic, defined as

$$SPE = \|\mathbf{Z} - \hat{\mathbf{Z}}\|_{\mathbb{H}}^2,$$

where $\hat{\mathbf{Z}} = \sum_{l=1}^{L^{\text{mon}}} \xi_l^{\text{mon}} \boldsymbol{\psi}_l^{\text{mon}}$.

Under the assumption of multivariate normality of ξ_l^{mon} , which is approximately true by the central limit theorem (Nomikos and MacGregor, 1995), the control limits of the Hotelling's T^2 control chart can be obtained by considering the $(1 - \alpha^*)$ quantiles of chi-squared distribution with L^{mon} degrees of freedom (Johnson et al., 2014). Whereas, the control limit for the SPE control chart can be computed by using the following equation (Jackson and Mudholkar, 1979)

$$CL_{SPE, \alpha^*} = \theta_1 \left[\frac{c_{\alpha^*} \sqrt{2\theta_2 h_0^2}}{\theta_1} + 1 + \frac{\theta_2 h_0 (h_0 - 1)}{\theta_1^2} \right]^{1/h_0}$$

where c_{α^*} is the $(1 - \alpha^*)$ -quantile of the standard normal distribution, $h_0 = 1 - 2\theta_1\theta_3/3\theta_2^2$, $\theta_j = \sum_{l=L^{\text{mon}}+1}^{\infty} (\lambda_l^{\text{mon}})^j$, $j = 1, 2, 3$. Note that α^* should be appropriately chosen to control the family wise error rate (FWER) denoted by α . We use the Šidák correction $\alpha^* = 1 - (1 - \alpha)^{1/2}$ (Šidák, 1967), which is exact for independent tests.

3 Simulation Study

The performance of the RoMFCC in identifying mean shifts of the multivariate functional quality characteristic is assessed through a Monte Carlo simulation of two scenarios with different Phase I sample contamination and data generation process (detailed in Supplementary Material A) inspired by typical behaviors of DRCs appeared in the real-case study of Section 4. Specifically, in Scenario 1 and Scenario 2, the Phase I sample is contaminated by functional cellwise and casewise outliers, respectively, with a contamination probability equal to 0.05 in both cases. Supplementary Material B reports additional results obtained with a contamination probability equal to 0.1. For each scenario, two contamination models, referred to as Out-E and Out-P, with three increasing contamination levels, referred to as C1, C2, and C3, are considered to mimic typical outlying DRCs. Specifically, Out-E mimics a splash weld (expulsion) caused by excessive welding current, while Out-P resembles the phase shift of the peak time caused by an increased force applied to the electrode used in the welding process (Xia et al., 2019). A further Scenario 0, simulates a Phase I sample not contaminated by any type of outliers. The Phase II sample is generated with two types of OC conditions at 4 different severity levels $SL = \{1, 2, 3, 4\}$, referred to as OC-E and OC-P coherently with contamination models Out-E and Out-P, respectively.

The proposed RoMFCC framework is compared with several natural competing approaches grouped into control charts for multivariate non-functional and functional data. The first group consists of control charts for multivariate data built on the mean vector of each component of multivariate functional data observations. In this group, we consider (i) the classical *multivariate* Hotelling's T^2 control chart, referred to as MCC; (ii) its *iterative* variant, referred to as iterMCC, where outliers detected by the control chart in Phase I are iteratively removed and control limits are revised until all data are assumed to be IC; (iii) the *multivariate robust* control chart proposed by Chenouri et al. (2009) and referred to as RoMCC. In the second group, we consider two approaches recently appeared in the profile monitoring literature, namely (iv) the *multivariate functional control chart* and referred to as MFCC, proposed by Capezza et al. (2020); (v) its *iterative* variant, referred to as iterMFCC, where, as before, outliers detected in Phase I are iteratively removed until all data are assumed to be IC.

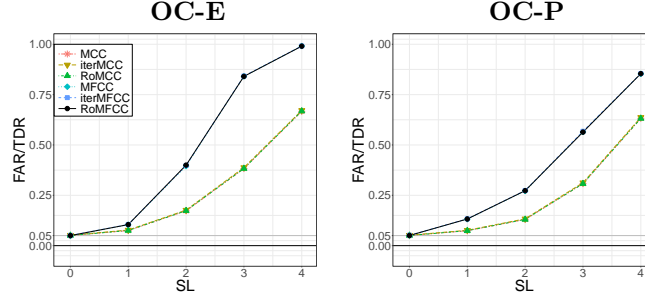
Scenario	Phase I				Phase II	
	Phase I contamination type	Contamination probability	Contamination model	Contamination level	OC condition type	SL
0	No contamination	-	-	-	OC-E, OC-P	0, 1, 2, 3, 4
1	Functional cellwise outliers	0.05, 0.01	Out-E, Out-P	C1, C2, C3	OC-E, OC-P	0, 1, 2, 3, 4
2	Functional casewise outliers	0.05, 0.01	Out-E, Out-P	C1, C2, C3	OC-E, OC-P	0, 1, 2, 3, 4

Table 1: Phase I generation scenarios and Phase II OC condition settings for the comparison of RoMFCC with competing methods.

The RoMFCC is implemented as described in Section 2 with $\delta_{fil} = \delta_{imp} = 0.999$ and $\delta_{mon} = 0.7$, and, to take into account the noise increase due to single imputation, five differently imputed datasets are generated through RoMFDI. While data are observed through noisy discrete values, each component of the generated quality characteristic observations is obtained by Equation (1) with $K = 10$ cubic B-splines estimated through the spline smoothing approach with a roughness penalty on the second derivative (Ramsay and Silverman, 2005). For each Phase I sample generation scenario and Phase II OC condition setting, 50 simulation runs are performed. Each run considers a Phase I random sample of 4000 observations. In particular, for MFCC, iterMFCC and RoMFCC, 1000 are used as a training set, and the remaining 3000 are used as a tuning set. The Phase II sample is also composed of a random sample of 4000 observations. The RoMFCC and the performance of the competing method are assessed through the true detection rate (TDR) and the false alarm rate (FAR), which are estimated as the average proportion, over the simulation runs, of points that fall outside the control limits whilst the process is, respectively, OC or IC. The latter are hereinafter referred to as mean TDR and mean FAR, respectively. The mean FAR should be as similar as possible to the overall type I error probability α considered to obtain the control limits and set equal to 0.05 in this simulation study, whereas the mean TDR should be as large as possible.

Figure 3 through 5 display for Scenario 0, Scenario 1, and Scenario 2, respectively, the mean FAR and TDR as a function of the severity level SL , at each OC condition type, contamination model and contamination level, as reported in Table 1. For Scenario 0, where the Phase I sample is not contaminated by outliers, Figure 3 shows that all the approaches that are able to account for the functional nature of the data (namely MFCC, iterMFCC, RoMFCC) achieve the same performance for both OC condition types.

Figure 3: Mean FAR ($SL = 0$) or TDR ($SL \neq 0$) achieved by MCC, iterMCC, RoMCC, MFCC, iterMFCC and RoMFCC for each OC condition (OC-E and OC-P) as a function of the severity level SL in Scenario 0. All the functional approaches (namely MFCC, iterMFCC, RoMFCC) plot equally and above the non-functional approaches (namely MCC, iterMCC, RoMCC) that also plot indistinctly.

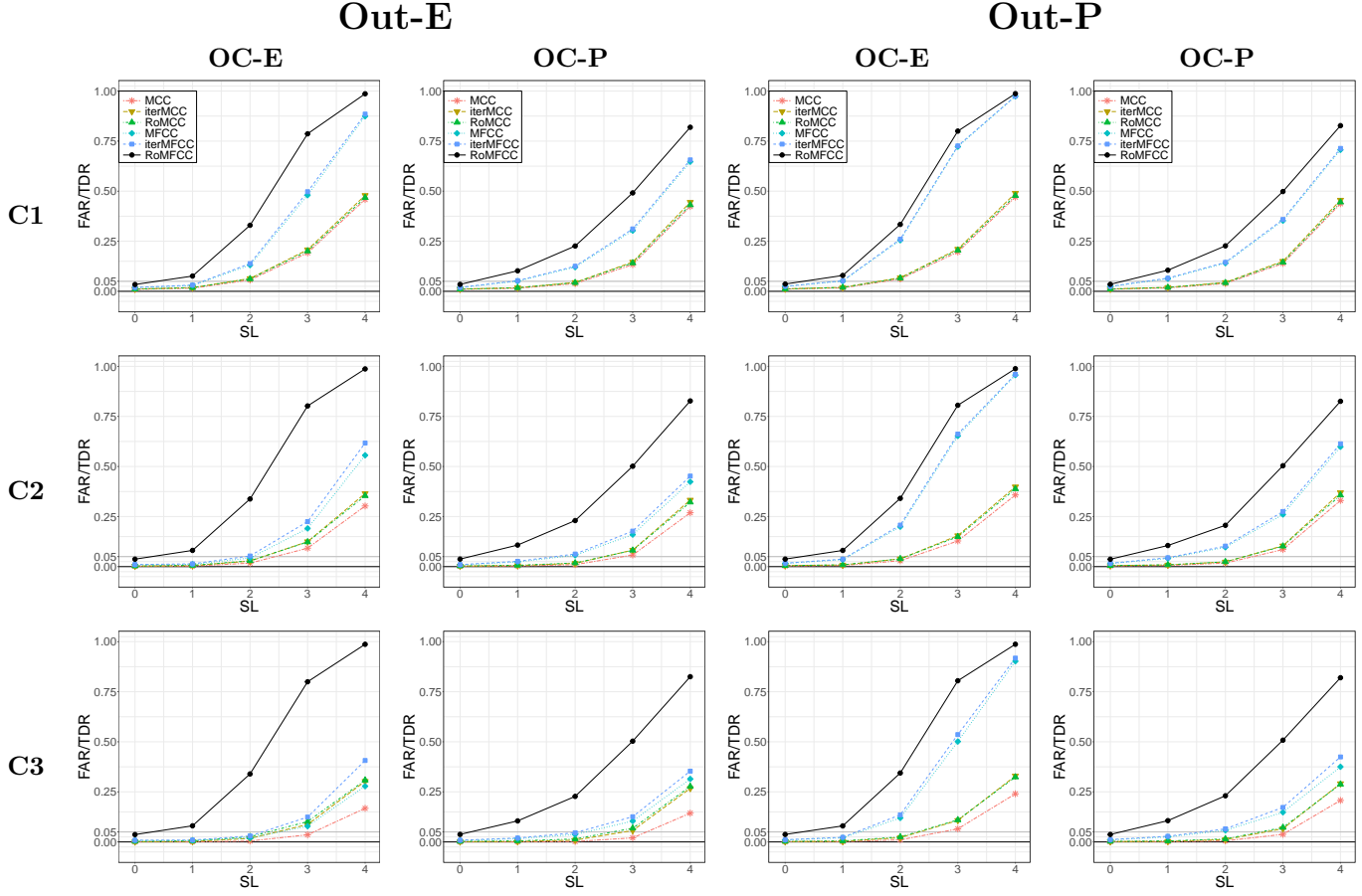


Although this scenario should be not favourable for approaches specifically designed to deal with outliers, iterMFCC and RoMFCC perform equal to MFCC. All the non-functional approaches (namely MCC, iterMCC, RoMCC) show instead worse performance than the functional counterparts and no significant differences among themselves.

In Scenario 1, the proposed RoMFCC is shown by Figure 4 to outperform all the competing methods for each contamination model, level and OC condition type. In particular, the larger the contamination level, the more the RoMFCC outperforms the competing methods. In fact, the performance of RoMFCC is insensitive to contamination models and levels, whereas the performance of the competing methods decreases with the contamination level for each contamination model, especially for Out-E. Regarding the non-robust functional methods (namely MFCC and iterMFCC), it turns out that the iterMFCC, which is expected to be the best competitor, does not really outperform MFCC. Moreover, their advantages over non-functional approaches decreases with the contamination level. The unsatisfactory performance of the non-functional methods reveals their inadequacy in jointly dealing with the functional nature of the data cellwise outliers.

As in Scenario 1, Figure 5 shows that the RoMFCC turns out to be the best method also in Scenario 2, although the performance difference with the competing methods is sometimes less pronounced. This is expected because in this scenario the Phase I sample is only contaminated by functional casewise outliers, which is the only contamination type the competing methods are designed to be robust against. Note that the performance of RoMFCC is in fact practically unaffected by outlier contamination also in this scenario. This completes the proof of the superiority of the proposed method in dealing not only

Figure 4: Mean FAR ($SL = 0$) or TDR ($SL \neq 0$) achieved in Phase II by MCC, iterMCC, RoMCC, MFCC, iterMFCC and RoMFCC for each contamination level (C1, C2, and C3), OC condition (OC-E and OC-P) as a function of the severity level SL with contamination model Out-E and Out-P and contamination probability 0.05 in Scenario 1.



with cellwise but also casewise outliers.

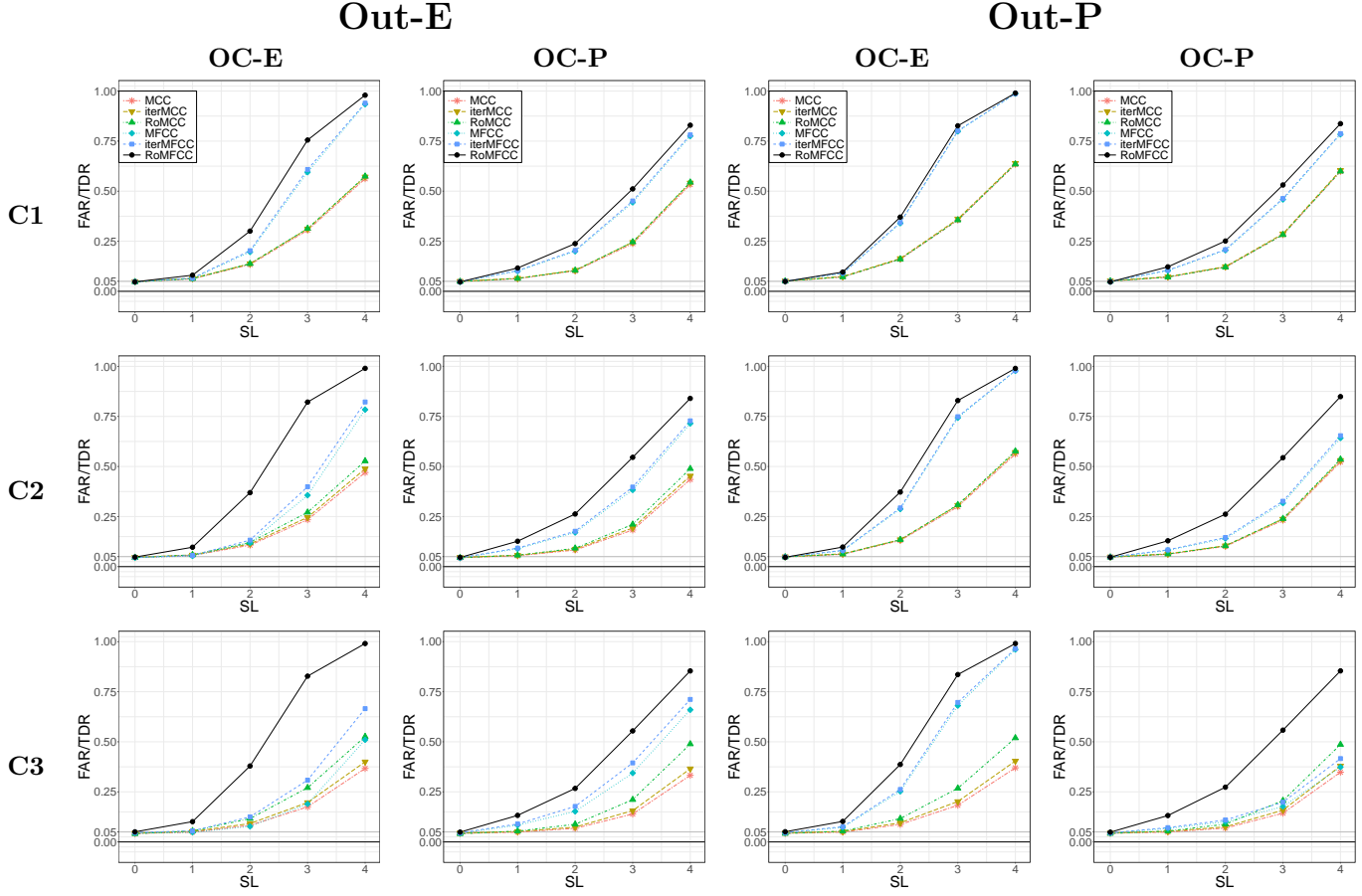
4 Real-Case Study

To demonstrate the potential of the proposed RoMFCC in practical situations, a real-case study in the automotive industry is presented henceforth. As introduced in Section 1, it addresses the issue of monitoring the quality of the RSW process, which is an autogenous welding process in which two overlapping conventional steel galvanized sheets are joint together, without the use of any filler material (Zhang and Senkara, 2011).

guarantees the structural integrity and solidity of welded items (Martín et al., 2014).

Joints are formed by applying pressure to the weld area from two opposite sides by means of two copper electrodes. Voltage applied to the electrodes generates a current flowing

Figure 5: Mean FAR ($SL = 0$) or TDR ($SL \neq 0$) achieved in Phase II by MCC, iterMCC, RoMCC, MFCC, iterMFCC and RoMFCC for each contamination level (C1, C2 and C3), OC condition (OC-E and OC-P) as a function of the severity level SL with contamination model Out-E and Out-P and contamination probability 0.05 in Scenario 2.



between them through the material. The electrical current flows because the resistance offered by metals causes significant heat generation (Joule effect) that increases the metal temperature at the faying surfaces of the work pieces up to the melting point. Finally, due to the mechanical pressure of the electrodes, the molten metal of the jointed metal sheets cools and solidifies, forming the so-called weld nugget (Raoelison et al., 2012). Further details on how the typical behaviour of a DRC is related to the physical and metallurgical development of a spot weld are provided in Capezza et al. (2021b).

Data analyzed in this study are courtesy of Centro Ricerche Fiat and are recorded during automotive body-in-white lab tests. This stage is generally characterized by a large number of spot welds with different characteristics, e.g, the thickness and material of the sheets to be joined together and the welding time. Specifically, this real-case study focuses on the monitoring of ten spot welds made by only one welding machine. In particular,

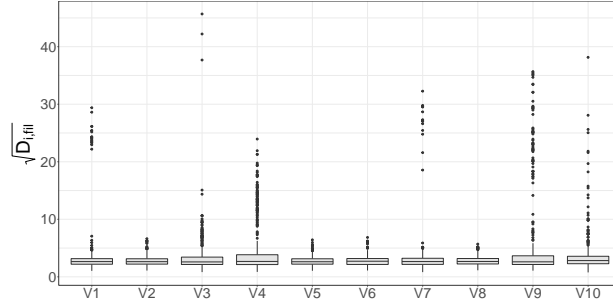


Figure 6: Boxplot of the functional distance square roots $\sqrt{D_{i,fil}}$ (Equation (3)) obtained from the FUF applied on the 460 Phase I observation of the training set.

for each item we consider the multivariate functional quality characteristic represented by the vector of ten DRCs relative to the same ten spot welding points, normalized on the time domain $[0, 1]$. The data set contains a total number of 1839 items and resistance measurements were collected at a regular grid of points equally spaced by 1 ms.

The RSW process quality is directly affected by electrode wear that leads to changes in electrical, thermal and mechanical contact conditions at electrode and metal sheet interfaces (Manladan et al., 2017). For this reason, electrodes are subjected to periodical tip dressing. Thus, a critical issue is the swift identification of DRCs mean shifts caused by electrode wear as a criterion to guide the electrode tip dressing program. To this aim, 919 observations of the multivariate functional quality characteristic corresponding to spot welds made immediately before electrode tip dressing are used to form the Phase I sample. The remaining 920 observations are used in Phase II to compare the in-line monitoring performance of the proposed RoMFCC with that of competing methods. The RoMFCC is implemented as in Section 3, where 460 Phase I observations, which are randomly selected without replacement, are used as training set and the remaining 459 ones as tuning set. Figure 6 shows the boxplot of the functional distance square root $\sqrt{D_{i,fil}}$ (Equation (3)) obtained from the FUF applied on the 460 Phase I observation of the training set. This figure confirms the outlier contamination in the training set, as already illustrated by Figure 1 for 100 randomly sampled DRCs.

Figure 7 shows the Hotelling's T^2 and SPE control charts of the RoMFCC framework for the real-case study data set. The vertical line separates the monitoring statistics calculated for the tuning set, on the left, and the Phase II sample on the right, while the control

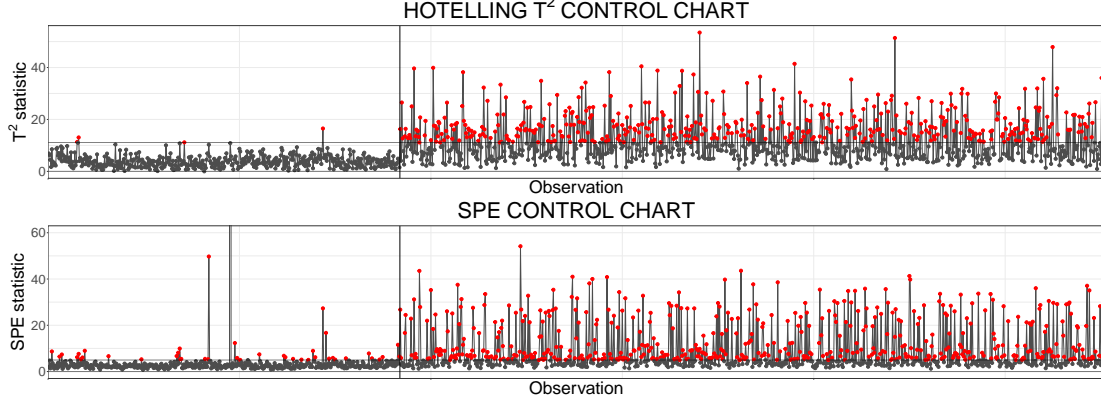


Figure 7: Hotelling's T^2 and SPE control charts of the RoMFCC framework for the real-case study data set. The vertical line separates the monitoring statistics calculated for the tuning set, on the left, and the Phase II sample, on the right, while the control limits are shown as horizontal lines.

limits are shown as horizontal lines. Note that the number of tuning set observations that plot above the control limits is expected because these points may include functional casewise outlier not filtered out by the FUF. In Phase II, the RoMFCC signals 72.3% of the observations as OC, which reflects the proposed method performance in tracking mean shifts caused by electrode wear.

Finally, the proposed method is compared with the competing methods presented in the simulation study of Section 3 through the estimated TDR, denoted as \widehat{TDR} , on the Phase II sample, as shown in Table 2. As expected from the results in Section 3, the considered non-functional approaches (MCC, iterMCC and RoMCC) show worse performance than the functional counterparts (MFCC, iterMFCC and RoMFCC) because they are not able to satisfactorily capture the functional nature of the data. Moreover, robust approaches (RoMCC and RoMFCC) outperform the non-robust counterparts, that is the \widehat{TDR} achieved by RoMCC is larger than MCC and iterMCC, whereas the \widehat{TDR} achieved by RoMFCC is larger than MFCC and iterMFCC. The uncertainty of \widehat{TDR} is quantified through a bootstrap analysis (Efron and Tibshirani, 1994). Table 2 reports the mean of the empirical bootstrap distribution of \widehat{TDR} , denoted by \overline{TDR} , and the corresponding bootstrap 95% confidence interval (CI) for each monitoring method. Bootstrap 95% confidence intervals achieved by the RoMFCC are strictly above those of all considered monitoring approaches. Therefore, the proposed RoMFCC stands out as the best method to promptly identify OC conditions in the considered RWS process characterized by a Phase I sample contaminated by functional outliers.

		\widehat{TDR}	\overline{TDR}	CI
Non functional	MCC	0.336	0.335	[0.305,0.368]
	iterMCC	0.462	0.461	[0.428,0.496]
	RoMCC	0.513	0.512	[0.481,0.547]
Functional	MFCC	0.541	0.541	[0.511,0.574]
	iterMFCC	0.632	0.632	[0.595,0.664]
	RoMFCC	0.723	0.723	[0.695,0.753]

Table 2: Estimated TDR values, denoted as \widehat{TDR} , on the Phase II sample, mean of the empirical bootstrap distribution of \widehat{TDR} , denoted by \overline{TDR} , and the corresponding bootstrap 95% confidence interval (CI) for each monitoring method.

5 Conclusions

In this paper, we propose a new robust framework for the statistical process monitoring of multivariate functional data, referred to as *robust multivariate functional control chart* (RoMFCC).

To the best of the authors' knowledge, the RoMFCC is the first statistical process monitoring (SPM) framework for multivariate functional quality characteristic that is robust to functional casewise and cellwise outliers. Indeed, methods already present in the literature either apply robust approaches to multivariate scalar features extracted from the profiles or use diagnostic approaches on the multivariate functional data to iteratively remove outliers. However, the former are not able to capture the functional nature of the data, while the latter are not able to deal with functional cellwise outliers.

The performance of the RoMFCC framework is assessed through an extensive Monte Carlo simulation study and is compared with several competing monitoring methods for multivariate scalar data and multivariate functional data. The ability to estimate the distribution of the data without removing observations allows the RoMFCC to outperform the competitors in all the considered settings and to represent the only alternative in high-dimensional scenarios where most of the competing methods may even fail. The proposed method is suitable to monitor industrial processes where many functional variables are available and are possibly contaminated by outliers, as anomalies in the data acquisition and data collected during a fault in the process.

The practical applicability of the proposed method is illustrated through the real-case study that motivated this research and addressed the issue of monitoring the quality of a resistance spot-welding (RSW) process in the automotive industry through multivariate

observations of the dynamic resistance curves as the quality characteristic of interest. Also in this real-case study, the RoMFCC outperforms all the considered competitors in the identification of out-of-control state of the RSW process due to the excessive wear of the electrode used.

Supplementary Materials

The Supplementary Materials contain additional details about the data generation process in the simulation study (A), additional simulation results (B), as well as the R code to reproduce graphics and results over competing methods in the simulation study.

References

- Agostinelli, C., Leung, A., Yohai, V. J., and Zamar, R. H. (2015). Robust estimation of multivariate location and scatter in the presence of cellwise and casewise contamination. *Test*, 24(3):441–461.
- Alemán-Gómez, Y., Arribas-Gil, A., Desco, M., Elías, A., and Romo, J. (2022). Depthgram: Visualizing outliers in high-dimensional functional data with application to fmri data exploration. *Statistics in Medicine*.
- Alfaro, J. and Ortega, J. F. (2009). A comparison of robust alternatives to hotelling’s t^2 control chart. *Journal of Applied Statistics*, 36(12):1385–1396.
- Alqallaf, F., Van Aelst, S., Yohai, V. J., and Zamar, R. H. (2009). Propagation of outliers in multivariate data. *The Annals of Statistics*, pages 311–331.
- Arribas-Gil, A. and Romo, J. (2014). Shape outlier detection and visualization for functional data: the outliergram. *Biostatistics*, 15(4):603–619.
- Boente, G. and Salibián-Barrera, M. (2021). Robust functional principal components for sparse longitudinal data. *Metron*, 79(2):159–188.
- Branden, K. V. and Verboven, S. (2009). Robust data imputation. *Computational Biology and Chemistry*, 33(1):7–13.
- Cabana, E. and Lillo, R. E. (2021). Robust multivariate control chart based on shrinkage for individual observations. *Journal of Quality Technology*, pages 1–26.
- Capezza, C., Centofanti, F., Lepore, A., Menafoglio, A., Palumbo, B., and Vantini, S. (2021a). Functional regression control chart for monitoring ship CO_2 emissions. *Quality and Reliability Engineering International*, 38(3):1519–1537.
- Capezza, C., Centofanti, F., Lepore, A., Menafoglio, A., Palumbo, B., and Vantini, S. (2022). funcharts: Control charts for multivariate functional data in R.

- Capezza, C., Centofanti, F., Lepore, A., and Palumbo, B. (2021b). Functional clustering methods for resistance spot welding process data in the automotive industry. *Applied Stochastic Models in Business and Industry*, 37(5):908–925.
- Capezza, C., Lepore, A., Menafoglio, A., Palumbo, B., and Vantini, S. (2020). Control charts for monitoring ship operating conditions and CO_2 emissions based on scalar-on-function regression. *Applied Stochastic Models in Business and Industry*, 36(3):477–500.
- Centofanti, F., Colosimo, B. M., Grasso, M. L., Menafoglio, A., Palumbo, B., and Vantini, S. (2021a). Robust functional anova with application to additive manufacturing.
- Centofanti, F., Lepore, A., Menafoglio, A., Palumbo, B., and Vantini, S. (2021b). Functional regression control chart. *Technometrics*, 63(3):281–294.
- Chenouri, S., Steiner, S. H., and Variyath, A. M. (2009). A multivariate robust control chart for individual observations. *Journal of Quality Technology*, 41(3):259–271.
- Chiou, J.-M., Chen, Y.-T., and Yang, Y.-F. (2014). Multivariate functional principal component analysis: A normalization approach. *Statistica Sinica*, pages 1571–1596.
- Cuesta-Albertos, J. A. and Fraiman, R. (2006). Impartial trimmed means for functional data. *DIMACS Series in Discrete Mathematics and Theoretical Computer Science*, 72:121.
- Cuevas, A. and Fraiman, R. (2009). On depth measures and dual statistics. a methodology for dealing with general data. *Journal of Multivariate Analysis*, 100(4):753–766.
- Dickinson, D., Franklin, J., Stanya, A., et al. (1980). Characterization of spot welding behavior by dynamic electrical parameter monitoring. *Welding Journal*, 59(6):170.
- Efron, B. and Tibshirani, R. J. (1994). *An introduction to the bootstrap*. CRC press.
- Fraiman, R. and Muniz, G. (2001). Trimmed means for functional data. *Test*, 10(2):419–440.
- Grasso, M., Menafoglio, A., Colosimo, B. M., and Secchi, P. (2016). Using curve-registration information for profile monitoring. *Journal of Quality Technology*, 48(2):99–127.
- Happ, C. and Greven, S. (2018). Multivariate functional principal component analysis for data observed on different (dimensional) domains. *Journal of the American Statistical Association*, 113(522):649–659.
- Hubert, M., Rousseeuw, P. J., and Segaeert, P. (2015). Multivariate functional outlier detection. *Statistical Methods & Applications*, 24(2):177–202.
- Hubert, M., Rousseeuw, P. J., and Vanden Branden, K. (2005). Robpca: a new approach to robust principal component analysis. *Technometrics*, 47(1):64–79.
- Hyndman, R. J. and Shang, H. L. (2010). Rainbow plots, bagplots, and boxplots for functional data. *Journal of Computational and Graphical Statistics*, 19(1):29–45.
- Hyndman, R. J. and Ullah, M. S. (2007). Robust forecasting of mortality and fertility rates: A functional data approach. *Computational Statistics & Data Analysis*, 51(10):4942–4956.

- Jackson, J. E. and Mudholkar, G. S. (1979). Control procedures for residuals associated with principal component analysis. *Technometrics*, 21(3):341–349.
- Jensen, W. A., Birch, J. B., and Woodall, W. H. (2007). High breakdown estimation methods for phase i multivariate control charts. *Quality and Reliability Engineering International*, 23(5):615–629.
- Johnson, R. A., Wichern, D. W., et al. (2014). *Applied multivariate statistical analysis*, volume 6. Pearson London, UK:.
- Jolliffe, I. (2011). *Principal component analysis*. Springer.
- Kokoszka, P. and Reimherr, M. (2017). *Introduction to functional data analysis*. Chapman and Hall/CRC.
- Kordestani, M., Hassanvand, F., Samimi, Y., and Shahriari, H. (2020). Monitoring multivariate simple linear profiles using robust estimators. *Communications in Statistics-Theory and Methods*, 49(12):2964–2989.
- Kruger, U. and Xie, L. (2012). *Statistical monitoring of complex multivariate processes: with applications in industrial process control*. John Wiley & Sons.
- Lee, S., Shin, H., and Billor, N. (2013). M-type smoothing spline estimators for principal functions. *Computational Statistics & Data Analysis*, 66:89–100.
- Leung, A., Zhang, H., and Zamar, R. (2016). Robust regression estimation and inference in the presence of cellwise and casewise contamination. *Computational Statistics & Data Analysis*, 99:1–11.
- Little, R. J. and Rubin, D. B. (2019). *Statistical analysis with missing data*, volume 793. John Wiley & Sons.
- Locantore, N., Marron, J., Simpson, D., Tripoli, N., Zhang, J., Cohen, K., Boente, G., Fraiman, R., Brumback, B., Croux, C., et al. (1999). Robust principal component analysis for functional data. *Test*, 8(1):1–73.
- López-Pintado, S. and Romo, J. (2011). A half-region depth for functional data. *Computational Statistics & Data Analysis*, 55(4):1679–1695.
- Manladan, S., Yusof, F., Ramesh, S., Fadzil, M., Luo, Z., and Ao, S. (2017). A review on resistance spot welding of aluminum alloys. *The International Journal of Advanced Manufacturing Technology*, 90(1):605–634.
- Maronna, R. A., Martin, R. D., Yohai, V. J., and Salibián-Barrera, M. (2019). *Robust statistics: theory and methods (with R)*. John Wiley & Sons.
- Martín, Ó., Pereda, M., Santos, J. I., and Galán, J. M. (2014). Assessment of resistance spot welding quality based on ultrasonic testing and tree-based techniques. *Journal of Materials Processing Technology*, 214(11):2478–2487.
- Menafoglio, A., Grasso, M., Secchi, P., and Colosimo, B. M. (2018). Profile monitoring of probability density functions via simplicial functional pca with application to image data. *Technometrics*, 60(4):497–510.

- Moheghi, H., Noorossana, R., and Ahmadi, O. (2020). Phase i and phase ii analysis of linear profile monitoring using robust estimators. *Communications in Statistics-Theory and Methods*, pages 1–18.
- Montgomery, D. C. (2012). *Introduction to Statistical Quality Control*. Wiley.
- Nomikos, P. and MacGregor, J. F. (1995). Multivariate spc charts for monitoring batch processes. *Technometrics*, 37(1):41–59.
- Noorossana, R., Saghaei, A., and Amiri, A. (2011). *Statistical analysis of profile monitoring*, volume 865. John Wiley & Sons.
- R Core Team (2021). *R: A Language and Environment for Statistical Computing*. R Foundation for Statistical Computing, Vienna, Austria.
- Ramaker, H.-J., van Sprang, E. N., Westerhuis, J. A., and Smilde, A. K. (2004). The effect of the size of the training set and number of principal components on the false alarm rate in statistical process monitoring. *Chemometrics and intelligent laboratory systems*, 73(2):181–187.
- Ramsay, J. O. and Silverman, B. W. (2005). *Functional Data Analysis*. Springer.
- Raelison, R., Fuentes, A., Rogeon, P., Carre, P., Loulou, T., Carron, D., and Dechalotte, F. (2012). Contact conditions on nugget development during resistance spot welding of zn coated steel sheets using rounded tip electrodes. *Journal of Materials Processing Technology*, 212(8):1663–1669.
- Rocke, D. M. (1996). Robustness properties of s-estimators of multivariate location and shape in high dimension. *The Annals of statistics*, pages 1327–1345.
- Rousseeuw, P. J. (1984). Least median of squares regression. *Journal of the American statistical association*, 79(388):871–880.
- Rousseeuw, P. J. and Bossche, W. V. D. (2018). Detecting deviating data cells. *Technometrics*, 60(2):135–145.
- Sawant, P., Billor, N., and Shin, H. (2012). Functional outlier detection with robust functional principal component analysis. *Computational Statistics*, 27(1):83–102.
- Šidák, Z. (1967). Rectangular confidence regions for the means of multivariate normal distributions. *Journal of the American Statistical Association*, 62(318):626–633.
- Sinova, B., Gonzalez-Rodriguez, G., and Van Aelst, S. (2018). M-estimators of location for functional data. *Bernoulli*, 24(3):2328–2357.
- Tarr, G., Müller, S., and Weber, N. C. (2016). Robust estimation of precision matrices under cellwise contamination. *Computational Statistics & Data Analysis*, 93:404–420.
- Van Buuren, S. (2018). *Flexible imputation of missing data*. CRC press.
- Van Ginkel, J. R., Van der Ark, L. A., Sijtsma, K., and Vermunt, J. K. (2007). Two-way imputation: A bayesian method for estimating missing scores in tests and questionnaires, and an accurate approximation. *Computational Statistics & Data Analysis*, 51(8):4013–4027.

- Vargas, N. J. A. (2003). Robust estimation in multivariate control charts for individual observations. *Journal of Quality Technology*, 35(4):367–376.
- Xia, Y.-J., Su, Z.-W., Li, Y.-B., Zhou, L., and Shen, Y. (2019). Online quantitative evaluation of expulsion in resistance spot welding. *Journal of Manufacturing Processes*, 46:34–43.
- Zhang, H. and Senkara, J. (2011). *Resistance welding: fundamentals and applications*. CRC press.

Supplementary Materials to “Robust Multivariate Functional Control Charts”

arXiv:2207.07978v2 [stat.AP] 10 Jan 2023

Table 1. Bessel correlation function and parameter for data generation in the simulation study.

	ρ	ν
$J_\nu(z) = \left(\frac{ z }{2}\right)^\nu \sum_{j=0}^{\infty} \frac{(-(z /\rho)^2/4)^j}{j!\Gamma(\nu+j+1)}$	0.125	0

A Details on Data Generation in the Simulation Study

The data generation process is inspired by the real-case study in Section 4 and mimics typical behaviours of DRCs in a RSW process. The data correlation structure is generated similar to Centofanti et al. (2021); Chiou et al. (2014). The compact domain \mathcal{T} is set, without loss of generality, equal to $[0, 1]$ and the number components p is set equal to 10. The eigenfunction set $\{\psi_i\}$ is generated by considering the correlation function \mathbf{G} through the following steps.

1. Set the diagonal elements G_{ll} , $l = 1, \dots, p$ of \mathbf{G} as the *Bessel* correlation function of the first kind (Abramowitz and Stegun, 1964). The general form of the correlation function and parameter used are listed in Table 1. Then, calculate the eigenvalues $\{\eta_{lk}^X\}$ and the corresponding eigenfunctions $\{\vartheta_{lk}\}$, $k = 1, 2, \dots$, of G_{ll} , $l = 1, \dots, p$.
2. Obtain the cross-correlation function G_{lj} , $l, j = 1, \dots, p$ and $l \neq j$, by

$$G_{lj}(t_1, t_2) = \sum_{k=1}^{\infty} \frac{\eta_k}{1 + |l - j|} \vartheta_{lk}(t_1) \vartheta_{jk}(t_2) \quad t_1, t_2 \in \mathcal{T}. \quad (\text{A.1})$$

3. Calculate the eigenvalues $\{\lambda_i\}$ and the corresponding eigenfunctions $\{\psi_i\}$ through the spectral decomposition of $\mathbf{G} = \{G_{lj}\}_{l,j=1,\dots,p}$, for $i = 1, \dots, L^*$.

Further, L^* is set equal to 10. Let $\mathbf{Z} = (Z_1, \dots, Z_p)$ as

$$\mathbf{Z} = \sum_{i=1}^{L^*} \xi_i \psi_i. \quad (\text{A.2})$$

with $\boldsymbol{\xi}_{L^*} = (\xi_1^X, \dots, \xi_{L^*}^X)^T$ generated by means of a multivariate normal distribution with covariance $\text{Cov}(\boldsymbol{\xi}_{L^*}^X) = \mathbf{\Lambda}^{\mathbf{X}} = \text{diag}(\lambda_1, \dots, \lambda_{L^*})$.

Furthermore, let the mean process m

$$m(t) = 0.2074 + 0.3117 \exp(-371.4t) + 0.5284(1 - \exp(0.8217t)) \\ - 423.3 [1 + \tanh(-26.15(t + 0.1715))] \quad t \in \mathcal{T}. \quad (\text{A.3})$$

Note that, the mean function m is generated to resemble a typical DRC through the phenomenological model for the RSW process presented in Schwab et al. (2012). Then, the contamination models C_E and C_P , which mimics a splash weld (expulsion) and phase shift of the peak time, are respectively defined as

$$C_E(t) = \min \left\{ 0, -2M_E(t - 0.5) \right\} \quad t \in \mathcal{T}, \quad (\text{A.4})$$

and

$$C_P(t) = -m(t) - (M_P/20)t + 0.2074 \\ + 0.3117 \exp(-371.4h(t)) + 0.5284(1 - \exp(0.8217h(t))) \\ - 423.3 [1 + \tanh(-26.15(h(t) + 0.1715))] \quad t \in \mathcal{T}, \quad (\text{A.5})$$

where $h : \mathcal{T} \rightarrow \mathcal{T}$ transforms the temporal dimension t as follows

$$h(t) = \begin{cases} t & \text{if } t \leq 0.05 \\ \frac{0.55-M_P}{0.55}t - (1 + \frac{0.55-M_P}{0.55})0.05 & \text{if } 0.05 < t \leq 0.6 \\ \frac{0.4+M_P}{0.4}t + 1 - \frac{0.4+M_P}{0.4} & \text{if } t > 0.6, \end{cases} \quad (\text{A.6})$$

and M_E and M_P are contamination sizes. Then, $\mathbf{X} = (X_1, \dots, X_p)^T$ is obtained as follows

$$\mathbf{X}(t) = \mathbf{m}(t) + \mathbf{Z}(t)\sigma + \boldsymbol{\varepsilon}(t) + B_E \mathbf{C}_E(t) + B_P \mathbf{C}_P(t) \quad t \in \mathcal{T}, \quad (\text{A.7})$$

where \mathbf{m} is a p dimensional vector with components equal to m , $\sigma > 0$, $\boldsymbol{\varepsilon} = (\varepsilon_1, \dots, \varepsilon_p)^T$, where ε_i are white noise functions such that for each $t \in [0, 1]$, $\varepsilon_i(t)$ are normal random variables with zero mean and standard deviation σ_e , and B_{CaE} and B_{CaP} are two indepen-

Table 2. Parameters used to generate the Phase I sample in Scenario 1 and Scenario 2 of the simulation study.

	Scenario 1				Scenario 2			
	Out-E		Out-P		Out-E		Out-P	
	$p_{CaE} = p_{CaP} = 1,$ $p_{CeE} = \tilde{p}, p_{CeP} = 0$		$p_{CaE} = p_{CaP} = 1,$ $p_{CeE} = 0, p_{CeP} = \tilde{p}$		$p_{CaE} = \tilde{p}, p_{CaP} = 0,$ $p_{CeE} = p_{CeP} = 1$		$p_{CaE} = 0, p_{CaP} = \tilde{p},$ $p_{CeE} = p_{CeP} = 1$	
	M_E	M_P	M_E	M_P	M_E	M_P	M_E	M_P
C1	0.04	0.00	0.00	0.40	0.02	0.00	0.00	0.20
C2	0.06	0.00	0.00	0.45	0.03	0.00	0.00	0.30
C3	0.08	0.00	0.00	0.50	0.04	0.00	0.00	0.40

Table 3. Parameters used to generate the Phase II sample for OC-E and OC-P and severity level $SL = \{0, 1, 2, 3, 4\}$ in the simulation study.

SL	OC-E		OC-P	
	$p_{CaE} = 1, p_{CaP} = 0,$ $p_{CeE} = 1, p_{CeP} = 0$		$p_{CaE} = 0, p_{CaP} = 1,$ $p_{CeE} = 0, p_{CeP} = 1$	
	M_E	M_P	M_E	M_P
	0	0.00	0.00	0.00
1	0.01	0.00	0.00	0.20
2	0.02	0.00	0.00	0.27
3	0.03	0.00	0.00	0.34
4	0.04	0.00	0.00	0.40

dent random variables following Bernoulli distributions with parameters p_{CaE} and p_{CaP} , respectively. Moreover, $\mathbf{C}_E = (B_{1,CeE}C_E, \dots, B_{p,CeE}C_E)^T$ and $\mathbf{C}_P = (B_{1,CeP}C_P, \dots, B_{p,CeP}C_P)^T$, where $\{B_{i,CeE}\}$ and $\{B_{i,CeP}\}$ are two sets of independent random variables following Bernoulli distributions with parameters p_{CeE} and p_{CeP} , respectively.

Then, the Phase I and Phase II samples are generated through Equation (A.7) by considering the parameters listed in Table 2 and Table 3, respectively, with $\sigma_e = 0.0025$ and $\sigma = 0.01$. The parameter \tilde{p} is the probability of contamination that for the data analysed in Section 3 and Supplementary Material B is set equal to 0.05 and 0.1, respectively. Moreover, in Scenario 0 of the simulation study data are generated through $p_{CaE} = p_{CaP} = p_{CeE} = p_{CeP} = 0$. Finally, the generate data are assumed to be discretely observed at 100 equally spaced time points over the domain $[0, 1]$.

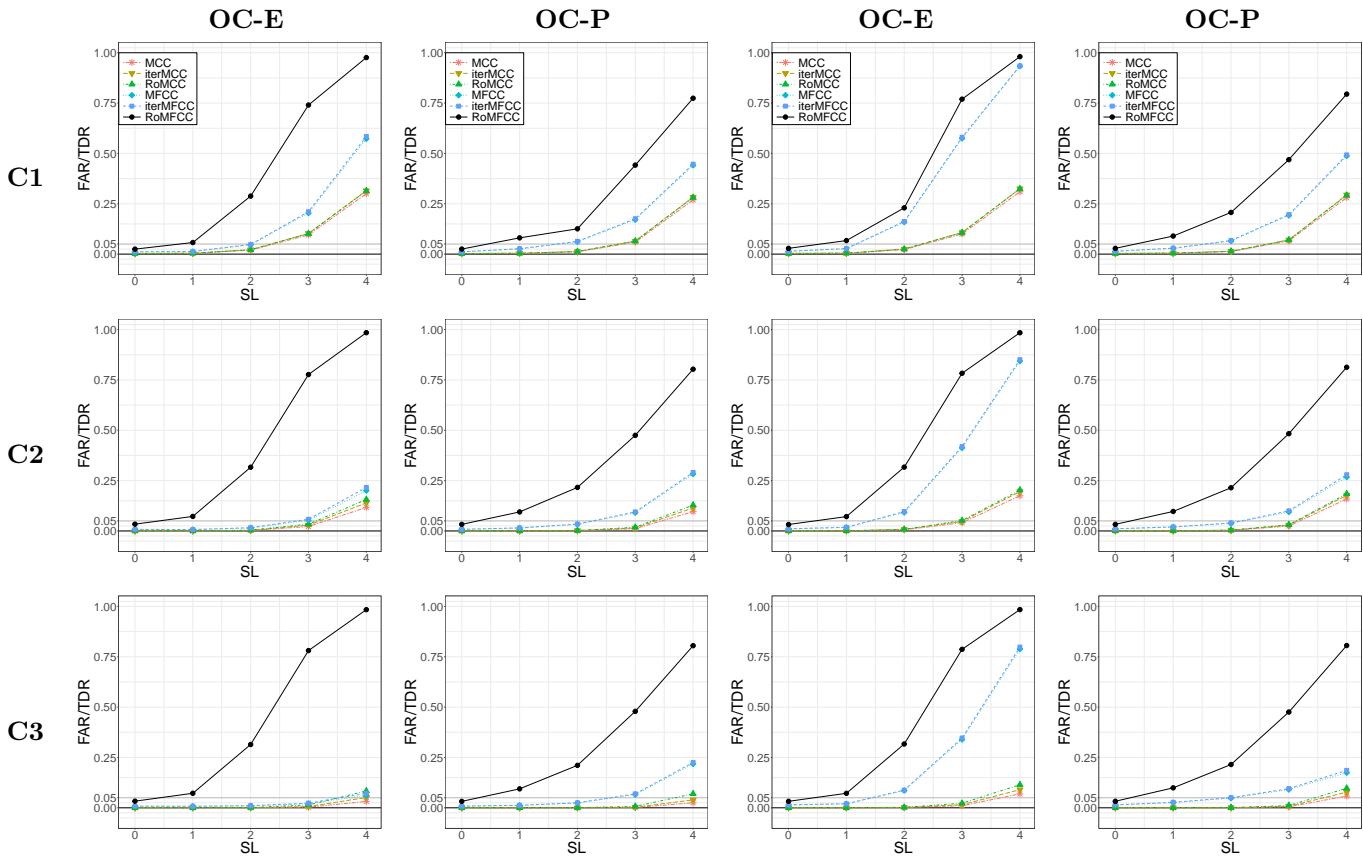
B Additional Simulation Results

In this section, we present additional simulations to analyse the performance of the RoMFCC and the competing methods methods when data are generated as described in Supplementary Material A with probability of contamination \tilde{p} equals to 0.1. The RoMFCC is implemented as described in Section 2. Figure A.1 and Figure A.2 show for Scenario 1 and Scenario 2 the mean FAR ($SL = 0$) or TDR ($SL \neq 0$) achieved by MCC, iterMCC, RoMCC, MFCC, MFCCiter and RoMFCC for each contamination level (C1, C2 and C3), OC condition (OC-E and OC-P) as a function of the severity level SL with contamination model Out-E and Out-P.

Figure A.1. Mean FAR ($SL = 0$) or TDR ($SL \neq 0$) achieved by MCC, iterMCC, RoMCC, MFCC, MFCCiter and RoMFCC for each contamination level (C1, C2 and C3), OC condition (OC-E and OC-P) as a function of the severity level SL with contamination model Out-E and Out-P in Scenario 1 for $\tilde{p} = 0.1$.

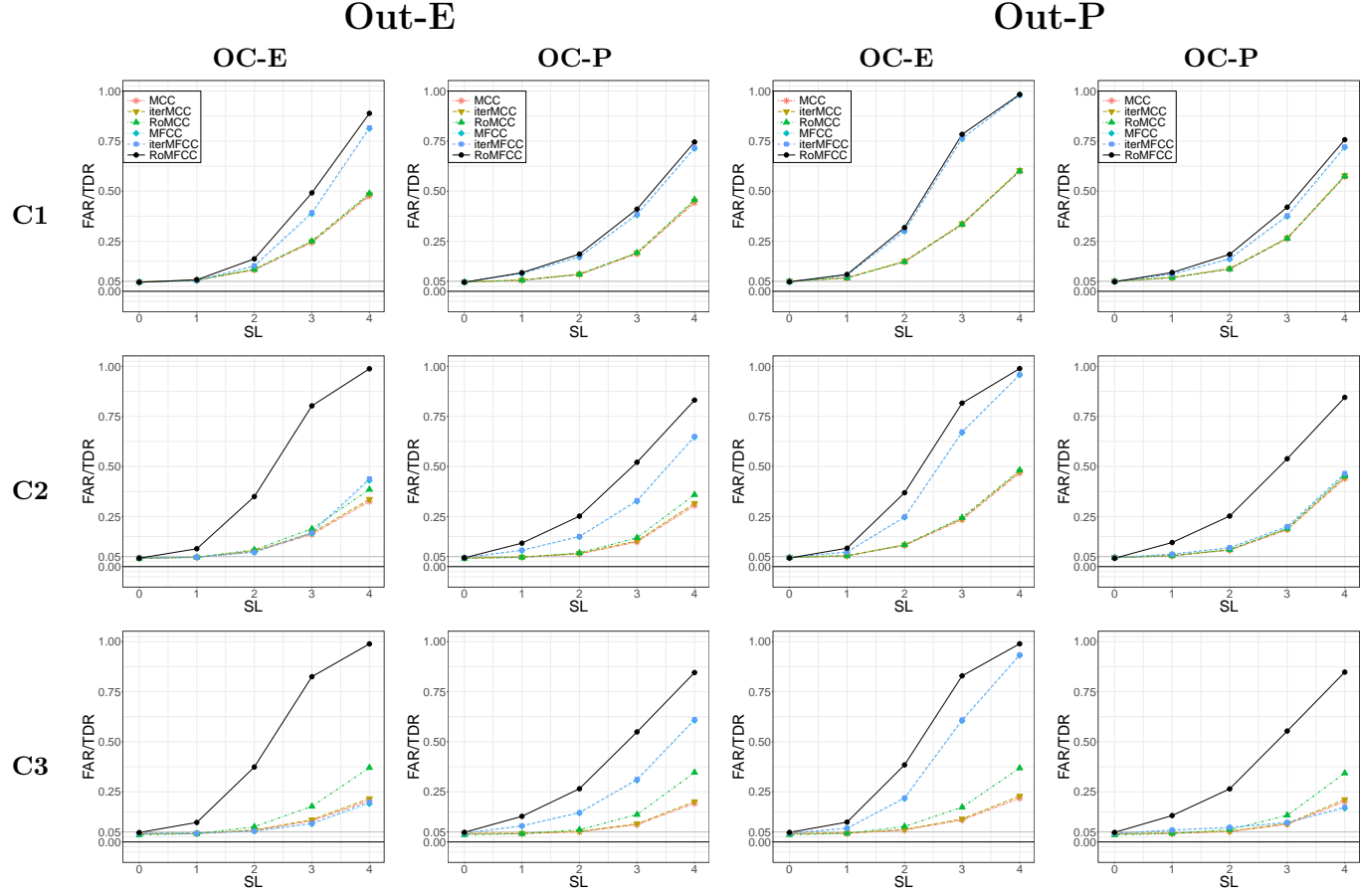
Out-E

Out-P



By comparing Figure A.1 and Figure A.2 with Figure 4 and Figure 5, the RoMFCC confirms itself as the best method in all the considered settings. Specifically, the proposed method, differently from the competing methods, is almost insensible to the fact that a

Figure A.2. Mean FAR ($SL = 0$) or TDR ($SL \neq 0$) achieved by MCC, iterMCC, RoMCC, MFCC, MFCCiter and RoMFCC for each contamination level (C1, C2 and C3), OC condition (OC-E and OC-P) as a function of the severity level SL with contamination model Out-E and Out-P in Scenario 2 for $\tilde{p} = 0.1$.



large fraction of the data in the Phase I sample is now composed by either cellwise or case wise outliers. On the contrary, the competing methods are strongly affected by the different probability of contamination and show overall worse performance than in Section 3 and, thus, are totally inappropriate to monitor the multivariate functional quality characteristic in this setting. This further confirms as shown in Section 3, i.e., in this simulation study the RoMFCC performance is almost independent of the contamination of the Phase I sample.

As in Section 3, also in this case, performance differences between the proposed and competing methods are less pronounced in Scenario 2 due to the less severe contamination produced by functional casewise outliers. However, RoMFCC still outperforms all the coming methods and, thus, stand out as the best method.

References

- Abramowitz, M. and I. A. Stegun (1964). Handbook of mathematical functions: with formulas, graphs, and mathematical tables.
- Centofanti, F., A. Lepore, A. Menafoglio, B. Palumbo, and S. Vantini (2021). Functional regression control chart. *Technometrics* 63(3), 281–294.
- Chiou, J.-M., Y.-T. Chen, and Y.-F. Yang (2014). Multivariate functional principal component analysis: A normalization approach. *Statistica Sinica*, 1571–1596.
- Schwab, I., M. Senn, and N. Link (2012). Improving expert knowledge in dynamic process monitoring by symbolic regression. In *2012 Sixth International Conference on Genetic and Evolutionary Computing*, pp. 132–135. IEEE.